Supporting information for the article

Measurement of nanoplasmonic field enhancement with ultrafast photoemission

Péter Rácz[1,‡], Zsuzsanna Pápa,[2,3,‡], István Márton[1], Judit Budai[2,3], Piotr Wróbel[4], Tomasz Stefaniuk[4], Christine Prietl[5], Joachim R. Krenn[5] and Péter Dombi[1,2,]*

[1] MTA "Lendület" Ultrafast Nanooptics Group, Wigner Research Centre for Physics, 1121 Budapest, Hungary
[2] ELI-ALPS Research Institute, ELI-HU Nonprofit Kft., 6720 Szeged, Hungary
[3] Department of Optics and Quantum Electronics, University of Szeged, 6720 Szeged, Hungary
[4] Faculty of Physics, University of Warsaw, 02-093 Warsaw, Poland
[5] Institut für Physik, Karl-Franzens Universität Graz, 8010 Graz, Austria

[‡]these authors contributed equally
*E-mail: dombi.peter@wigner.mta.hu

1. Experimental methods

We employed two types of sample fabrication methods. (i) Gold nanoparticle arrays containing typically ~70,000 nanoparticles were fabricated with standard electron beam lithography onto fused silica substrates covered with a 40 nm thick conductive indium-tin-oxide (ITO) layer. Scanning electron microscopy (SEM) images of these samples supporting localized plasmon modes at the femtosecond laser wavelength of ~800 nm are shown in Figs. 2(a) and (b) of the main article. (ii) Silver thin film samples supporting propagating surface plasmons, featuring 0.7 and 4.7 nm root-mean-square roughness were produced by electron beam evaporation of Ag with precisely controlled temperature and wetting layers. Details of this thin film fabrication method are given in Refs. [1,2].

Femtosecond laser illumination of all of these samples was performed (i) with a home-built long-cavity Ti:sapphire oscillator directly delivering 175-nJ laser pulses at 792 nm central wavelength with 95 fs pulse length close to the transform limit of the oscillator spectrum [3]. The repetition rate was reduced to 4.5 kHz with an extracavity electrooptic pulse picker in order to avoid overlap between the signals of subsequent laser pulses in the time-of-flight spectrometer. (ii) Alternatively, a regenerative Ti:sapphire amplifier was also used ("Legend Elite" from

Coherent Inc.) with 42-fs pulses delivered with 1 kHz repetition rate at 804 nm central wavelength. As evidenced by formula (1) of the main article, pulse length and repetition rate do not influence the measurement principle and process. In both cases, pulse energy was adjusted by a variable neutral density attenuator to achieve the desired peak intensity in the focus of the beam.

Electrons emitted from the plasmonic samples were characterized by a time-of-flight (TOF) spectrometer (designed and built by Kaesdorf GmbH) with a flight tube of 45 cm length. The sample glass plate or the Kretschmann-prism acted as the vacuum window of the TOF chamber with the plasmonic nanoparticle or thin film samples being at the vacuum side. The axis of the flight tube of the TOF spectrometer is normal to the surface of the sample where the nanoparticle array or the plasmonic thin film is situated (see Fig. 1. of the main article). Electron counts from a microchannel plate detector situated at the end of the magnetically shielded flight tube were recorded by a fast multiscaler card with 100 ps time resolution. The discrimination level for these signal pulses was set to 4 mV. After calibration, electrons having kinetic energies in the 3 eV to 200 eV range could be accurately measured with this setup. For each electron spectrum 200,000 to 2,500,000 electron counts were recorded, depending on the excitation intensity. For each spectrum electrons from 300,000 to 500,000 consecutive laser pulses were accumulated within a measurement time of 89 to 300 seconds.

2. Quiver amplitude of electrons in the nanooptical near-fields

It is known that the formula $Q_{\max} = 10.007\ e^2\lambda^2 E_{\mathrm{loc,max}}^2 / (16\ \pi^2 mc^2) + 0.538W$ for the maximum electron kinetic energy is only valid if the quiver amplitude of the photoemitted electron in the oscillating nanooptical field is less than the field decay length [4]. (m and e are the electron mass and charge, respectively, λ is the laser wavelength, E_{loc} is the local electromagnetic field, c is the speed of light and W is the work function of the metal.)

The quiver amplitude is given by $A = eE_{\mathrm{loc}}\,\lambda^2/(4\pi^2 mc^2)$ [4] and accordingly, we tabulated quiver amplitude values for the maximum focused intensity that we applied to each of the four different samples, considering also the measured field enhancement factor (f), i. e. $E_{\mathrm{loc,max}} = f\,E_{\mathrm{focus,max}}$. Corresponding results are given in Table S1.

Table S1. Maximum field enhancement factor, local field and electron quiver amplitude for the maximum focused laser intensity that was applied to each of the four different samples used for the experiments.

Sample name	Maximum focused intensity (GW/cm^2)	Maximum measured field enhancement factor	Maximum local field, $E_{loc,max}$ (V/nm)	Maximum electron quiver amplitude (nm)
Resonant nanorod	45.6	36.1	21.2	0.68
Resonant bowtie	25.1	50.5	22.0	0.70
Silver film with 0.7 nm roughness	224	21.0	27.3	0.88
Silver film with 4.7 nm roughness	161	30.8	33.9	1.09

It can be seen that maximum quiver amplitudes never exceeded 1.1 nm during our experiments. Field decay lengths, on the other hand, are typically above 10 nm for plasmonic nanostructures as evidenced e. g. by Fig. 3(e) of the main article. Even more so for propagating surface plasmons where decay lengths are known to reach some hundreds of nm [5], therefore all experiments were performed within the quiver regime, where the validity of the 10.007 prefactor in the formula for Q_{max} is upheld [4].

3. Details of the finite-difference time-domain simulations

We performed finite-difference time-domain (FDTD) simulations with a commercially available software package (Lumerical), both for propagating and localized plasmons. The simulated 3D unit cell (350 nm × 350 nm × 1000 nm for the nanorods and 650 nm × 350 nm × 1000 nm for the bowtie) in the case of localized plasmonic fields contained a gold nanostructure on top of a bulk fused silica substrate covered with an ITO layer. The substrate was modeled with constant refractive index $n = 1.45$. We determined the optical properties and the thickness of the ITO with an ellipsometric measurement ($\varepsilon' = 3.33$, $\varepsilon'' = 0.14$ and 40 nm thickness, respectively). For gold nanoparticles $\varepsilon' = -22.89$ and $\varepsilon'' = 0.75$ was used according to Ref. [6]. To ensure an accurate description of the nanoobjects' near-field, meshing with a unit size of 0.25 × 0.25 × 0.25 nm^3 was used in the area of the nanorod and bowtie apex. Periodic boundary conditions were

applied in the directions parallel with the substrate surface, and perfectly matched layer (PML) boundaries in the perpendicular direction.

Extinction spectra of the nanorod and the bowtie were calculated using a linearly polarized total-field scattered-field (TFSF) plane wave source. The absorbed and the scattered power were recorded inside and outside the source region by frequency domain field monitors to determine the near-field extinction spectra of the particles. The plasmon resonance of nanostructures forming a periodic grating can be influenced by near-field or far-field electromagnetic interaction between the particles. In the case of our samples, the nanoparticles form a grating structure with particle distances larger than the ones allowing near-field coupling, but they may interact via their dipole fields which interfere, forming collective radiation [7]. For this reason, the particle arrays were illuminated with a plane wave source having the same characteristics as the TFSF source, and the transmitted power was recorded by a frequency domain field monitor placed 50 nm above the nanostructure. We used a far-field projection option to calculate the response of the nanostructure array in the far-field. Extinction curves determined by far-field simulations were later compared with the measured ones (Figs. S1(e) and (f)).

Since individual nanoparticle geometries within the arrays cannot be described by a single radius of curvature (R) value, but rather by a radius distribution, the effect of the variation of R on the calculated field enhancement values was investigated. The distribution of R values was determined by evaluating several SEM images for the nanorod and bowtie nanoparticles (Figs. S1(a) and (b)). Field enhancement calculations were performed at different values of R. The obtained values as a function of R are plotted in Figs. S1(c) and (d). Our results show that field enhancement slightly increases with decreasing R values, as expected. Final results presented in the main text are the ones belonging to the maxima of the distributions. Since the histogram of the bowties has two, almost equal radius-of-curvature maxima, we applied the R = 11 nm value for the simulations for which higher maximum kinetic energies are expected. Our simulation geometry and results were validated by comparing simulation data to optical spectroscopic characterization (extinction curves) of the nanorod and bowtie arrays. This comparison resulted in well matching resonance curves as shown in Figs. S1(e) and (f).

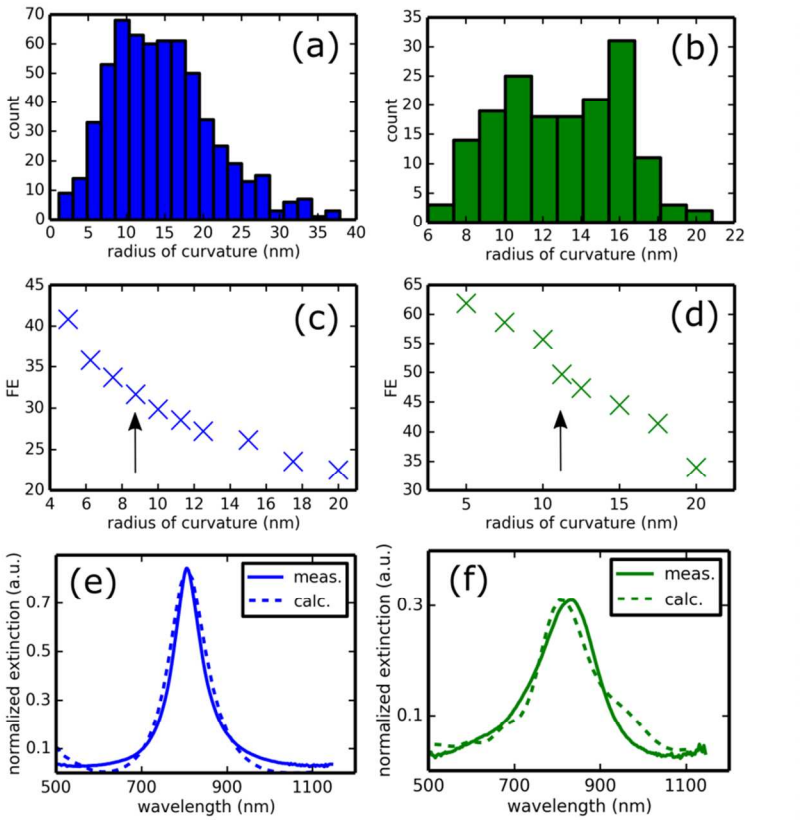

Figure S1 (a) and (b) The distribution of radius-of-curvature values determined according to SEM images for the nanorod and bowtie nanoparticles, respectively. (c) and (d) Results of the field enhancement calculations for different values of *R* in the case of nanorods and bowties. Arrows point to field enhancement values presented in the main article, corresponding to (local) maxima of the histograms. (e) and (f) The extinction curves of nanorod (e) and bowtie (f) structures obtained from the experiments (solid line) and from the simulations (dashed line).

The uncertainty of the simulation results was estimated based on the variation of the geometrical parameters of the individual nanoobjects. Beside the radius of curvature, we measured the length distribution of the nanorods and bowties, showing a variation of less than 3%. Performing simulations with the different geometrical parameters, it turned out that the radius of curvature variation has the largest impact on the computed field enhancement values. The field enhancement belonging to different *R* values (Figs. S1 (c) and (d)) were fitted with a polynomial function in order to calculate the field enhancement of each *R* value, and standard deviations were calculated for these datasets. The obtained standard deviations in field enhancement are 5.3 and 5.8 for nanorod and bowtie arrays, respectively.

The surface of the nanoobjects is not perfectly smooth. According to SEM images, the grain size of the gold structures is around 15 nm (see Fig. S2(a)). To describe the effect of the surface inhomogeneities of the nanorods, surface roughness was introduced to the model with 15 nm correlation length and 1 nm rms roughness (Fig. S2(b)). This small roughness has a negligible effect on the simulated extinction curve as it was also shown, for example by Ref. [8]. The calculated field distribution near the nanorod apex is presented in Fig. S2(c). The maximum value of the field enhancement is 34.5 in this case. Comparing this value to the one obtained in the case of nanorods with perfectly smooth surface (31.7), it can be seen that the deviation is within 10%. This difference mainly originates from the surface areas with slightly smaller radius of curvature.

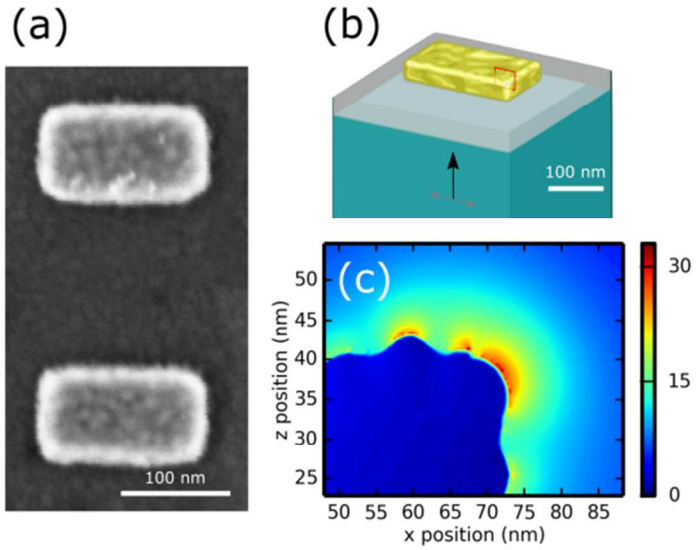

Figure S2 (a) SEM image of the nanorods used for modeling nanoparticle roughness. (b) Scheme of the simulated rough nanorod. The black arrow shows the incidence of a linearly polarized plane wave with the polarization direction indicated by the grey arrows. Grey area indicates the 40-nm indium-tin-oxide layer whereas blue indicates the fused silica substrate. The red rectangles show the area of the field distribution map in (c). The field enhancement near the apices of the nanorod reaches a maximum value of 34.5.

For modeling surface roughness for propagating plasmons, representative areas with 300 nm × 300 nm lateral size were chosen from AFM images recorded on the samples (Figs. S3(a) and (b), rms roughnesses of 0.7 nm and 4.7 nm, respectively). These areas were chosen so that the size of the central nanostructure in the images coincides with the maximum of the structure size distributions presented in Figs. S3(c) and (d) for the two different roughness values. The silver layer thickness was set at 50 nm. The optical properties of the fused silica substrate

were described with constant refractive index (n = 1.45). We used optical constants of silver that were measured on samples deposited under the same conditions as our samples under study [2], resulting in ε' = -30.07 and ε'' = 1.98 for the smoother surface and ε' = -30.07 and ε'' = 0.90 for the rougher surface. Periodic boundary conditions were applied in the directions parallel to the substrate surface, and PML boundaries containing 60 layers in the perpendicular direction.

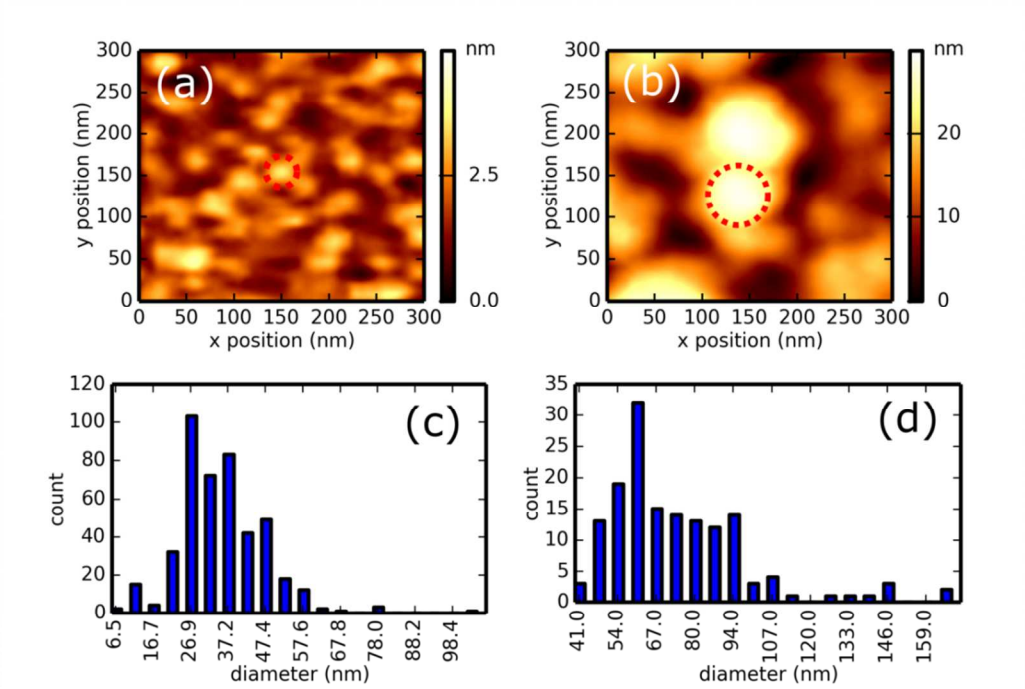

Figure S3 (a) and (b) Representative areas of AFM images recorded on the plasmonic silver surfaces with 0.7 nm and 4.7 nm rms roughness, respectively. (c) and (d) Surface grain size distributions for the corresponding silver surfaces.

The uncertainty of the simulation results was estimated (similarly to the nanoparticle arrays) based on the variation of the grain size distributions of the silver surfaces. The field enhancement values were determined at several grains in the vicinity of the ones marked with red dashed circles in Figs. S3(a) and (b)). The field enhancement values plotted against grain diameter were fitted with a polynomial function, and the field enhancement was calculated for each grain according to the fitting. The standard deviations of these datasets are 1.3 for the plasmonic silver surface with 0.7 nm rms roughness and 6.4 for the surface with 4.7 nm rms roughness.

In order to validate the simulation setup, the reflectivity of the nanostructured samples was calculated at different angles of incidence. The accurate modeling of these rough surfaces requires excessively long simulation times, therefore the incidence angles corresponding to

reflection minima were determined from simulations of smaller regions with less accurate mesh settings. Since positions of the obtained reflection minima (44.6° and 44.8°) coincide with the measured angular resonance curves in Figs. 2(g) and (h) of the main article, the presented field enhancement values were calculated at these angles of incidence with a 3D non-uniform mesh with step sizes between 0.25 and 0.5 nm in the region of the rough silver surface. This value was small enough to properly describe the shape of the nanostructures.

The field distributions were recorded by 3D frequency domain field and power monitors enabling us to plot the field distributions of different viewpoints. Figs. S4(a) and (b) show the rough surfaces, with the red rectangles representing monitor planes parallel to the substrate surface. Field maps in these planes are shown by Figs. S4(c) and (d) confirming again the maximum field enhancement values.

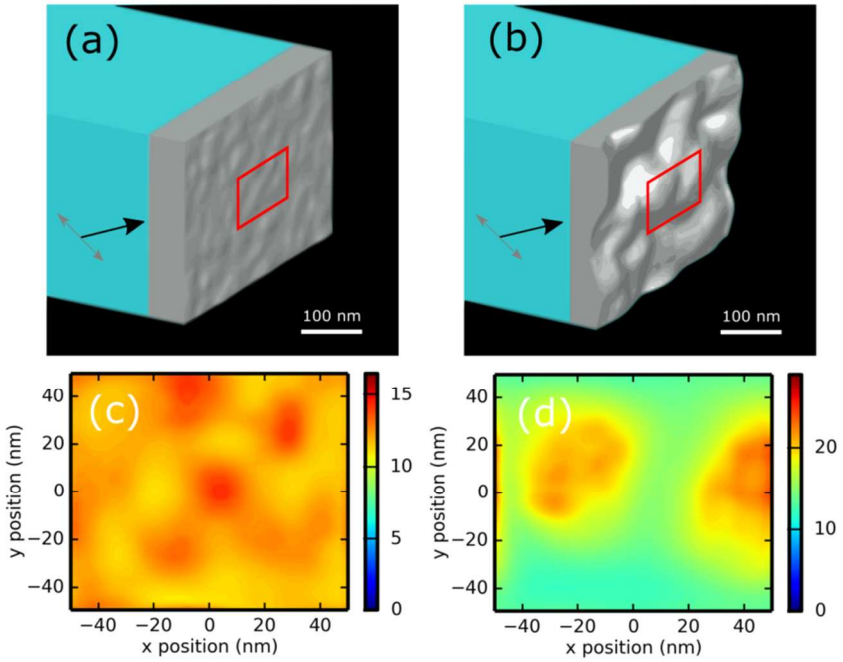

Figure S4 (a) and (b) Scheme of the rough plasmonic surfaces with 0.7 nm (a) and 4.7 nm (b) rms roughness. Red rectangles represent the monitor areas. (c) and (d) Field distributions in the corresponding monitor areas.

The FDTD simulation parameters given above were set according to a strict convergence check. During this process, we checked the mesh settings, the distance between the PML boundary and the monitors, the number of the PML layers and the simulation time window. Fig. S5 shows the dependence of the obtained field enhancement values on the mesh size for the

nanorod and the rough silver surface with 0.7 nm rms roughness. The mesh step applied for simulations presented in the main text were always chosen as the best tradeoff between the accuracy and the simulation time/memory requirements.

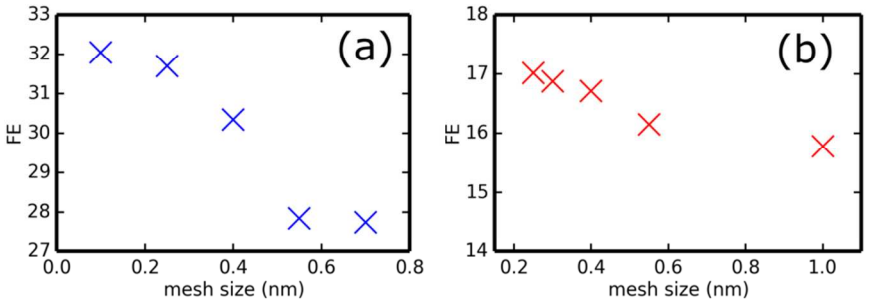

Figure S5 The dependence of the obtained field enhancement values on the mesh density for (a) nanorod and (b) rough plasmonic surface with 0.7 nm rms roughness.

4. References

[1] Stefaniuk, T.; Wróbel, P.; Trautman, P.; Szoplik T. *Appl. Opt.* **2014**; 53, B237-B241.

[2] Wróbel, P.; Stefaniuk, T.; Trzcinski, M.; Wronkowska, A. A.; Wronkowski, A.; Szoplik, T. *ACS Appl. Mater. Interfaces* **2015** ; 7, 8999–9005.

[3] Dombi, P.; Rácz, P.; Lenner, M.; Pervak, V.; Krausz, F. *Opt. Express* **2009**; 17, 20598-20604 and references therein.

[4] Herink, G.; Solli, D. R.; Gulde, M.; Ropers C. *Nature* **2012**, 483, 190-193.

[5] Raether, H.: *Surface Plasmons on Smooth and Rough Surfaces and on Gratings,* Springer Berlin Heidelberg, **1988**.

[6] Haynes, W. M. (Ed.): *CRC Handbook of Chemistry and Physics, 96th Edition*, CRC Press Taylor and Francis Group, Boca Raton FL, **2015**.

[7] Lamprecht, B.; Schider, G.; Lechner, R. T.; Ditlbacher, H.; Krenn, J. R.; Leitner, A.; and Aussenegg, F. R. *Phys. Rev. Lett.* **2000**; 84, 4721-4724.

[8] Trügler, A.; Tinguely, J.-C.; Krenn, J. R.; Hohenau, A.; and Hohenester, U. *Phys. Rev. B* **2011;** 83, 081412 1-4.